Journal of Ceramic Processing Research. Vol. 20, No. 6, pp. 577~581 (2019)
(Received 14 November 2018, Received in revised form 17 January 2019, Accepted 9 May 2019)
https://doi.org/10.36410/jcpr.2019.20.6.577

J O U R N A L O F
Ceramic Processing Research

Optical and scintillation properties of Tb-doped apatite single crystals

Takayuki Yanagida* and Noriaki Kawaguchi
Devision of Materials Science, Nara Institute of Science and Technology, 8916-5 Takayama-cho, Ikoma, Nara 630-0101, Japan

In the present study, we focus on the Tb-doped Sr-based apatite materials which have a chemical composition of $Sr_2RE_8(SiO_4)_6O_2$ where RE denotes the rare earth element. The target materials in this study were Tb 0.5% doped $Sr_2Gd_8(SiO_4)_6O_2$, $Sr_2Y_8(SiO_4)_6O_2$, $Sr_2(Gd_{0.5}Lu_{0.5})_8(SiO_4)_6O_2$ and $Sr_2(Gd_{0.4}Lu_{0.6})_8(SiO_4)_6O_2$ crystals, and they were synthesized by the floating zone method. When we checked powder X-ray diffraction patter, we confirmed a single phase (JCPDS No:28-0212) for all the samples. In photoluminescence (PL) and X-ray induced scintillation spectra, some sharp emission lines appeared, and the emission origin was Tb^{3+} 4f-4f transition. We investigated PL and scintillation decay time profiles, and the main component was 1.8 and 1.3 ms, respectively. Among the samples prepared here, $Sr_2Gd_8(SiO_4)_6O_2$ showed the highest scintillation intensity.

Key words: Scintillator, Scintillation detector, Ionizing radiation, Luminescence.

Introduction

Scintillators are one of the luminescent materials which have a function to absorb the ionizing radiation and emit UV-Vis photons [1-4]. The spectrum of the application of scintillators are side, including medical imaging [5], security [6], well-logging [7], environmental monitoring [8], high energy physics [9]. In the recent trend, scintillator materials consist of a host and an emission center, as same as the other phosphor materials. The main function of the host is to absorb the target ionizing radiation efficiently, and that of the emission center is to emit UV-Vis photons. The combination (chemical composition) of the host and emission center is important so many materials have been developed and examined for scintillator uses.

Rare earth elements have been used both for the host and the emission center in scintillation materials, and common examples for scintillators are Ce-doped $(Y,Gd,Lu)_2SiO_5$ [10-12] and $(Y,Gd,Lu)_3(Al,Ga)_5O_{12}$ [13-15]. In these materials, the combination of the host and emission centers is efficient, and luminous scintillation can be achieved. In addition to Ce-doped rare earth host materials, Pr^{3+} [16] and Tb^{3+} [17] are sometimes selected as the emission centers in scintillators. In this work, we focus Tb^{3+} as an emission center since the number of study of Tb-doped scintillators is limited when we compare with Ce- or Pr-doped materials.

As a host material, we focus on the apatite crystals. The apatite crystals are represented as $RE_{9.33}(SiO_4)_6O_2$ and $AE_2RE_8(SiO_4)_6O_2$, where *RE* and *AE* denote rare earth and alkaline earth elements, respectively. As can be seen in the composition, apatite crystals can contain a certain amount of rare earth ions, and a high stopping power against high energy photons can be expected if *RE* is Gd or Lu. In general, apatite materials are applied in medicine such as artificial born [18] and other applications [19-20]. Up to now, we have synthesized and evaluated Ce-doped apatite crystals [21-25], and we think the combination of apatite host and Tb^{3+} emission centers would be interesting.

In the present study, we focus on the Tb-doped Sr-based apatite materials which have a chemical composition of $Sr_2RE_8(SiO_4)_6O_2$ (RE = rare earth element). Up to now, we have investigated Ce-doped apatite crystalline scintillators [21-25], and there still remains a large room for study for other emission centers. Tb 0.5 % doped $Sr_2Gd_8(SiO4)_6O_2$, $Sr_2Y_8(SiO_4)_6O_2$, $Sr_2(Gd_{0.5}Lu_{0.5})_8(SiO_4)_6O_2$ and $Sr_2(Gd_{0.4}Lu_{0.6})_8(SiO_4)_6O_2$ crystals were synthesized by the floating zone method to investigate optical and scintillation properties. When we compare the floating zone method with other common melt growth techniques, we do not have to use crucibles in the floating zone method, and it is quite advantageous in viewpoints of the growth cost and avoiding unexpected contamination. Typical speed of the crystal growth is also attractive in the floating zone method, and we can grow few mmf × few cm crystal in 6-8 hours. On the other hand, to grow a big crystal is generally difficult in this method, and if a big crystal is required, conventional Czochralski or Bridgeman method will be better. Hereafter, we call $Sr_2Gd_8(SiO_4)_6O_2$, $Sr_2Y_8(SiO_4)_6O_2$, $Sr_2(Gd_{0.5}Lu_{0.5})_8(SiO_4)_6O_2$ and $Sr_2(Gd_{0.4}Lu_{0.6})_8(SiO_4)_6O_2$ as SrGS, SrYS, SrGdLuS (Gd:Lu=1:1), and SrGdLuS (Gd:Lu=3:2).

*Corresponding author:
Tel : +81-743-72-6144
Fax: +82-743-72-6147
E-mail: t-yanagida@ms.naist.jp

Experimental

0.5% Tb-doped SrGS, SrYS, SrGdLuS (Gd:Lu=1:1), and SrGdLuS (Gd:Lu=2:3) apatite crystal of $(Gd_{0.4}Lu_{0.6})_8Sr_2(SiO_4)_6O_2$ were synthesized by the floating zone method. First, raw material powders of Tb_4O_7, Y_2O_3, Gd_2O_3, Lu_2O_3, $SrCO_3$ and SiO_2 were mixed by using mortar and pestle. Next, the mixture powder was heated at 1100 °C for 10 h so as to remove CO_2 from $SrCO_3$. Then, the obtained mixture powder was formed to a cylinder by a hydrostatic pressure. All the cylinder rods of the powder mixtures were sintered at 1500 °C for 12 h to make ceramic rods. Finally, a ceramic rod was loaded into an FZ furnace (FZD0192, Canon Machinery Inc.) to synthesize a crystal under ambient atmosphere. Here, the pull-down rate was approximately 3 mm/h, and the rotation rate was 20 rpm.

The crystalline structures of the synthesized samples were identified by XRD using a diffractometer (MiniFlex600, Rigaku). After we grew crystal samples, the samples were partially crashed to obtain a powder to investigate the phase of the samples. The XRD patterns were evaluated in the 2θ range from 20 to 60°.

As optical properties, PL excitation and emission contour graphs were measured by using Quantaurus-QY (Hamamatsu), and at the same time, we also evaluated the PL *QY* in all the samples. The PL decay times were evaluated with Quantaurus-t (Hamamatss) with the time correlated single photon counting technique. The excitation and monitoring wavelengths were 265 and 540 nm, respectively. Since the excitation source was pulsed white light source, we used an optical filter which could transmit photons from 255 to 275 nm (the center wavelength was 265 nm). In the monitoring side, we put a bandpass filter of which transmitted wavelength was from 510 to 570 nm (the center wavelength was 540 nm). In addition, a short cut filter (< 470 nm) was automatically set in the instrument to cut the excitation photons.

X-ray induced radioluminescence (RL), or scintillation, spectra were measured using a lab-constructed set-up [26] as described below. X-rays from the X-ray generator was delivered directly to the sample. The consequent emission as RL was guided, through an optical fibre, monochromator (SR163, ANDOR), and finally to the CCD (DU920-BU2NC, ANDOR) to measure the spectrum. Here, the applied voltage and current to the X-ray tube was fixed to 60 kV and 1 mA, respectively. The scintillation decay time profile was measured by using our original setup [27], which is equipped with a pulse X-ray tube.

Results and Discussion

Fig. 1 represents appearances of the grown crystals. Although there have been many cracks in the grown crystals, we can obtain partially transparent samples. If we increase the ratio of Lu in Lu and Gd mixed materials, we could not obtain a single crystal sample. Therefore, the maximum Lu ratio in this series would be around 60%, and this result was also confirmed in our recent work about Ce-doped apatite crystals [22]. In order to measure optical and scintillation properties, we cut relatively transparent and less-crack part.

Fig. 2 represents powder XRD patterns of the samples. We confirmed that all the crystals did not have any impurity phases within the detection limit of XRD measurement, and the XRD patterns well coincided with the standard data of $Ca_2Gd_8(SiO_4)_6O_2$ (JCPDS No:28-0212). Peak angles of Tb:SrGdLuS, Tb:SrGdLuS, and Tb:SrYS were higher than that of Tb:SrGS. It can be explained by the difference in the lattice constants. When valences and coordination numbers of Lu, Y, and Gd are the same, ionic radii of Lu and Y are smaller than that of Gd. Therefore, the lattice constants of Tb:SrGdLuS, Tb:SrGdLuS, and Tb:SrYS, which contain Lu and Y, could be smaller than that of Tb:SrGS.

Fig. 3 represents PL excitation and emission contour graphs of all the samples. In all the samples, some emission lines due to Tb^{3+} 4f-4f transition were observed from 350 to 650 nm. The excitation wavelengths were the same in all the samples, and it was from 250 to 290

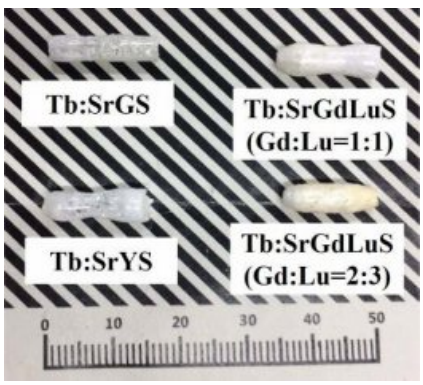

Fig. 1. Appearances of samples synthesized in this work.

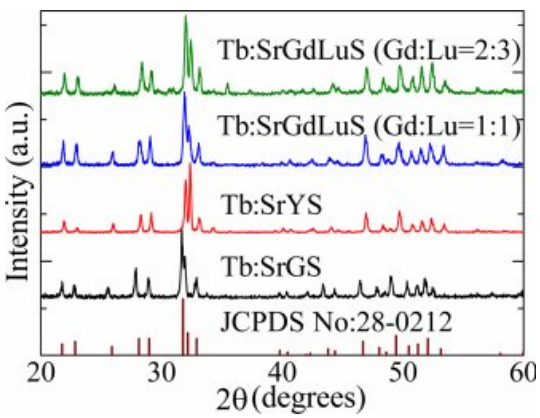

Fig. 2. Powder XRD patterns of the samples.

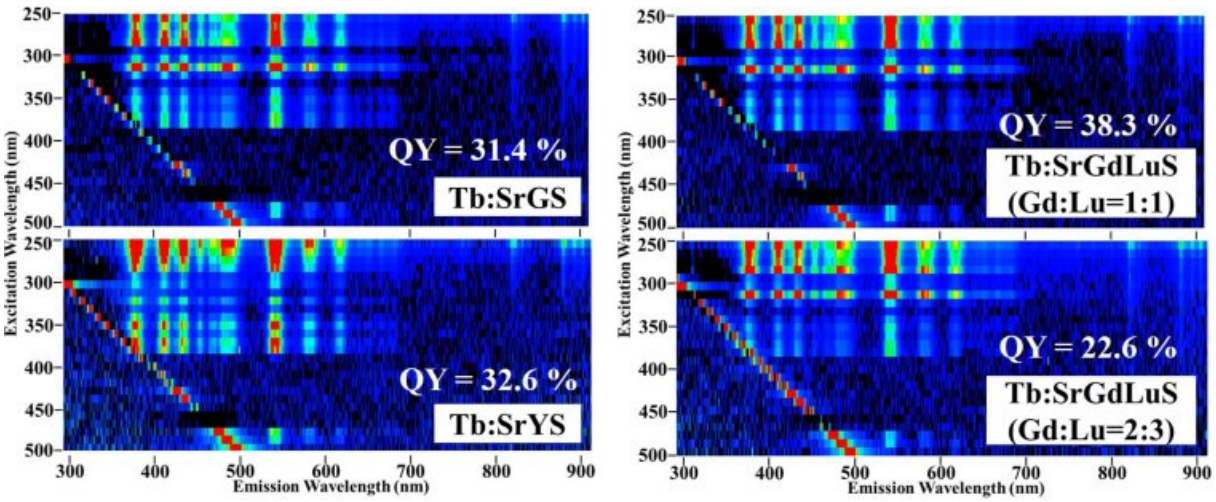

Fig. 3. PL excitation (horizontal axis) and emission (vertical axis) contour graphs of all the samples. The calculated *QY* is also shown in each panel.

nm. The emission lines at UV and visible lengths are caused by the electron transitions from $^5D_{3,4}$ excited states to ^7Fi_i ground states, and the observed spectral feature was typical as Tb-doped phosphors [28-30]. The PL *QY* are also written in the figure, and *QY* of SrGS, SrYS, SrGdLuS (Gd:Lu=1:1), and SrGdLuS (Gd:Lu= 2:3) were 31.4, 32.6, 38.3 and 22.6 %, respectively. All the samples had higher PL *QY* than Ce-doped apatite crystals which were previously investigated. Among the present samples tested here, SrGdLuS (Gd:Lu=1:1) showed the best PL *QY*, and the tendency was the same with Ce-doped $Sr_2(Gd_xLu_{1-x})_8(SiO_4)_6O_2$ crystals [22]. In this series of materials, the ratio of Gd:Lu = 1:1 may be optimum for the PL-based phosphor application.

Fig. 4 demonstrates PL decay time profiles of all the samples monitoring at 540 nm under 265 nm excitation. In the decay part, all the curves were well approximated by a single exponential function, and the decay times were typical for Tb^{3+} emission. The decay times of SrGS, SrYS, SrGdLuS (Gd:Lu=1:1), and SrGdLuS (Gd:Lu=2:3) resulted 1.86, 1.92, 1.78 and 1.75 ms, respectively. These PL decay times are typical in Tb-doped materials [31, 32]. On the other hand, if we focus on the rise part, all the samples showed a slow rise time. Generally, such a slow rise suggests a sign of an energy transfer phenomenon. Although there are several evaluation methodologies for the rise time, here, we adopt the 10 %-90 % method to determine the rise time by neglecting the spike like component which was due to the instrumental response (excitation pulse). As a result, the rise time of SrGS, SrYS, SrGdLuS (Gd:Lu=1:1), and SrGdLuS (Gd:Lu=2:3) were 0.25, 0.22, 0.24 and 0.25 ms, respectively. In Gd-containing samples, the energy transfer may be possible since the PL decay of Gd^{3+} 4f-4f transition is generally a few ms and excitation and emission wavelengths are ~270 and ~310 nm. In our materials, Gd^{3+} is one of the main components of the host (in other words, Gd 100 % doping), and some quenching would make the decay of Gd^{3+} faster (sub-ms). But such an interpretation is impossible for SrYS since it does not contain Gd^{3+}. The remaining possibility will be the energy transfer from the host-based emission to Tb^{3+}. In the past study, we observed the host luminescence of this series of apatite crystals with a broad band from 300 to 600 nm in X-ray induced RL spectrum [22-24], and the host emission overlapped with the excitation bands of Tb^{3+} (Fig. 3). Up to now, we have not succeeded to observe clear PL of the host emission due to the low emission intensity of undoped samples. From the present results, the excitation of the host emission of $AE_2RE_8(SiO_4)_6O_2$ may be around 265 nm. The other possible scenario is a multi-phonon relaxation which has been observed in the other Tb-doped materials [33].

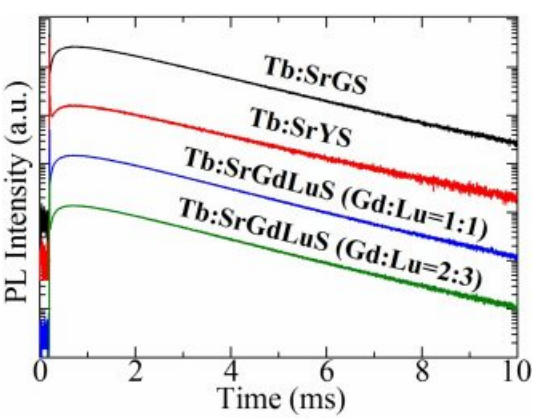

Fig. 4. PL decay time profiles of all the samples monitoring at 540 nm under 340 nm excitation.

Fig. 5 shows X-ray excited RL spectra of all the samples. As same as the PL spectra, some sharp lines due to 4f-4f transitions of Tb^{3+} appeared from 350 to

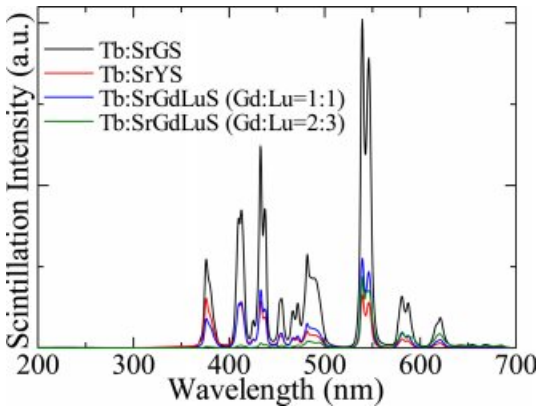

Fig. 5. X-ray induced RL spectra of all the samples.

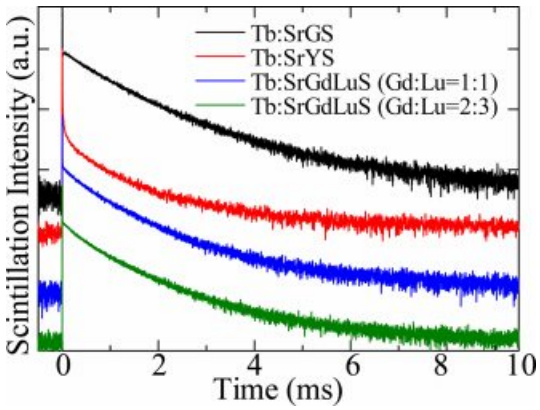

Fig. 6. X-ray induced scintillation decay time profiles of all the samples.

650 nm, and the electron transitions were from $^5D_{3,4}$ excited states to ^7Fi_i ground states. In this observation, the emission around 540 nm ($^5D_4 \rightarrow {}^7F_5$) showed the highest intensity in all the lines, and the same tendency was observed in the scintillation of Tb-doped some other materials such as BaY_2F_8 [34], $45SiO_2–10Al_2O_3–25BaO–(20−x)BaF_2$ glass [35], $LuBO_3$ [36] and some other materials. Although the RL is not a quantitative but a qualitative study, we can compare the emission intensity with the other $AE_2RE_8(SiO_4)_6O_2$ type apatite crystals with a similar size since the stopping power against X-rays is similar in materials with similar chemical composition. Among the present samples, Tb:SrGS exhibited the highest scintillation intensity, and when we compare with Ce-doped $AE_2RE_8(SiO_4)_6O_2$ type apatite crystals qualitatively, the scintillation intensity of present samples were higher.

Fig. 6 shows scintillation decay time profiles of all the samples. In the scintillation decay, all the curves were well approximated by a single exponential function, and the decay times were typical for Tb^{3+} emission. The scintillation decay times of SrGS, SrYS, SrGdLuS (Gd:Lu=1:1), and SrGdLuS (Gd:Lu=2:3) were 1.33, 1.28, 1.23, and 1.24, respectively. The scintillation decay was faster than PL decay, and the reason will be blamed for the quenching among the excited states. In scintillation, a large number of secondary electrons are excited, and the spatial scale of the dispersion of secondary electrons is around 100 nm [37]. In PL, we observe an excitation and relaxation of one electron within the bandgap, and we generally do not consider such an interaction between electrons except for the case of semiconductor materials. In such a case, interactions among excited electrons cannot be negligible, and such interactions sometimes arise a quenching phenomenon. Such a phenomenon is called a linear energy transfer (LET) effect or excitation density effect. Unlike PL, the slow rise was not observed, and the emission origin of the scintillation did not relate to the energy transfer.

Summary and Conclusions

We synthesized Tb-doped SrGS, SrYS, SrGdLuS (Gd:Lu=1:1), and SrGdLuS (Gd:Lu=2:3) by the floating zone method. In PL and scintillation, we observed some sharp emission lines due to Tb^{3+} 4f-4f transition from 350 to 650 nm. All the samples showed higher PL *QY* than those observed in Ce-doped apatite crystals which were previously reported. In the scintillation upon X-ray excitation, Tb-doped SrGS showed the highest emission intensity among the samples tested in this work. In PL and scintillation, decay times due to Tb^{3+} 4f-4f transition were 1.75-1.86 ms and 1.23-1.33 ms, respectively.

Acknowledgement

This work was supported by Grant-in-Aid for Scientific Research (A) (17H01375) and (B) (18H03468) from the Ministry of Education, Culture, Sports, Science and Technology of the Japanese government (MEXT), A-STEP from Japan Science and Technology Agency (JST). The Cooperative Research Project of Research Institute of Electronics, Shizuoka University, Terumo Foundation for Life Sciences and Arts, Izumi Science and Technology Foundation, The Kazuchika Okura Memorial Foundation, and The Iwatani Naoji Foundation are also acknowledged.

References

1. P. A. Rodniy, in “Physical Processes in Inorganic Scintillators” (CRC Press, 1997) p. 18.
2. G. Knoll, in “Radiation Detection and Measurement” (Wiley & Sons Hoboken Press, 2000) p. 223.
3. C.W.E. van Eijk, Nucl. Instrum. Methods Phys. Res. A 392[1-3] (1997) 285-290.
4. T. Yanagida, Proc. Jpn. Acad. B 94[2] (2018) 75-97.
5. K. Nakanishi, S. Yamamoto, H. Watabe, S. Abe, N. Fujita, andK. Kato, Nucl. Inst. and Meth. A 880 (2018) 118-124.
6. D. Mannes, F. Schmid, J. Frey, K. Schmidt-Ott, and E. Lehmann, Physics Procedia 69 (2015) 653-660.

7. T. Yanagida, Y. Fujimoto, S. Kurosawa, K. Kamada, H. Takahashi, Y. Fukazawa, M. Nikl, and V. Chani, Jpn. J. Appl. Phys. 52 (2013) 076401.
8. K. Watanabe, T. Yanagida, K. Fukuda, A. Koike, T. Aoki, and A. Uritani, Sens. Mater. 27 (2015) 269-275.
9. H. Takahashi, T. Yanagida, D. Kasama, T. Ito, M. Kokubun, K. Makishima, T. Yanagitani, H. Yagi, T. Shigeta, and T. Ito IEEE Trans. Nucl. Sci. 53[4] (2006) 2404-2408.
10. P.A. Cutler, C.L. Melcher, M.A. Spurrier, P. Szupryczynski, and L.A. Eriksson, IEEE Trans. Nucl. Sci. 56[3] (2009) 915-919.
11. C.L. Melcher and J.S. Schweitzer, IEEE Trans. Nucl. Sci. 39[4] (1992) 502-505.
12. P.L. Reeder, Nucl. Instrum. Methods Phys. Res. A 353[1-3] (1994) 134-136.
13. M. Moszynski, M. Kapusta, M. Mayhugh, D. Wolski, and S.O. Flyckt, IEEE Trans. Nucl. Sci., 44[3] (1997) 1052-1061.
14. A. Lempicki, M.H. Randles, D. Wisniewski, M. Balcerzyk, C. Brecher, and A.J. Wojtowicz, IEEE Trans. Nucl. Sci. 42[4] (1995) 280-284.
15. S. Yamamoto, J. Kataoka, T. Oshima, Y. Ogata, T. Watabe, H. Ikeda, Y. Kanai, and J. Hatazawa, Nucl. Instrum. Methods Phys. Res. A 821 (2016) 28-33.
16. Y. Wu and G. Ren, Opt. Mater. 35[12] (2013) 2146-2154.
17. I. Kandarakis and D. Cavouras, Applied Radiation and Isotopes 54[5] (2001) 821-831.
18. W. Brigitte and D.P. Jill, Mater. Sci. Eng. C 25 (2005) 131-143.
19. S. Qingle and H. Zhang, J. Rare Earths 30[12] (2012) 1235-1239.
20. X. Han, J. Lin, Z. Li, X. Qi, M. Li, and X. Wang, J. Rare Earths 26[6] (2008) 904-906.
21. T. Igashira, N. Kawano, G. Okada, N. Kawaguchi, and T. Yanagida, Optik 155 (2018) 36-42.
22. T. Igashira, N. Kawano, G. Okada, N. Kawaguchi, and T. Yanagida, Opt. Mater. 79 (2018) 232-236.
23. T. Igashira, N. Kawano, G. Okada, N. Kawaguchi, and T. Yanagida, J. Mater. Sci. Mater EL 28[24] (2017) 18630-18636.
24. T. Igashira, M. Mori, G. Okada, N. Kawaguchi, and T. Yanagida, Opt. Mater. 64 (2017) 239-244.
25. T. Igashira, M. Mori, G. Okada, N. Kawaguchi, and T. Yanagida, J. Rare Earths 35[11] (2017) 1071-1076.
26. T. Yanagida, K. Kamada, Y. Fujimoto, H. Yagi, and T. Yanagitani, Opt. Mater. 35[12] (2013) 2480-2485.
27. T. Yanagida, Y. Fujimoto, T. Ito, K. Uchiyama, and K. Mori, Appl. Phys. 7[6] (2014) 062401.
28. D. Sztolberg, B. Brzostowski, and P. J. Dereń, Opt. Mater. 78 (2018) 292-294.
29. A. Mendoud, L. Guerbous, A. Boukerika, B. Boudine, and N. Benrekaa, Opt. Mater. 75 (2018) 802-808.
30. S. Mahlik, F. Diaz, and P. Boutinaud, J. Lumin. 191 (2017) 18-21.
31. J.F.M. dos Santos, N.G.C. Astrath, M.L. Baesso, L.A.O. Nunes, and T. Catund, J. Lumin. 202 (2018) 363-369.
32. N. Wada and K. Kojima, Opt. Mater. 35 (2013) 1908-1913.
33. Q. Shi, F. You, S. Huang, H. Peng, Y. Huang, and Y. Tao, Chem. Phys. Lett. 601 (2014) 21-25.
34. A.C.S. de Melloa Adriano, B.A. Gerson, H.G. Nakamura, S.L. Baldochib Mário, and E.G. Valerio, Opt. Mater. 32[10] (2010) 1337-1340.
35. S. Jia, L. Huang, D. Ma, Z. Tai, S. Zhao, D. Deng, H. Wang, G. Jia, Y. Hua, Q. Yang, and S. Xu, J. Lumin. 152 (2014) 241-243.
36. C. Mansuy, J. M. Nedelec, C. Dujardin, and R. Mahiou, Opt. Mater. 29[6] (2007) 697-702.
37. M. Koshimizu, K. Asai, and H. Shibata, J. Lumin. 94-95 (2001) 407-411.